Proceedings of Korean Nuclear Society Spring Meeting
Kwangju, Korea, May 2002

Electrochemical Estimation on the Applicability of Nickel Plating to EAC Problems in CRDM Nozzle

Si Hyoung Oh, Il Soon Hwang

Seoul National University
56-1 Shinlim-dong, Gwanak-ku, Seoul, Korea
Phone +82-2-880-7200 Fax +82-2-3285-9600

Abstract

The applicability of nickel-plating to EAC problems in CRDM nozzle was estimated in the light of electrochemical aspect. The passive film growth law for nickel was improved to include oxide dissolution rate improving conventional point defect model to explain retarded passivation of plated nickel in PWR primary side water environment and compared with experimental data. According to this model, oxide growth and passivation current is closely related with oxide dissolution rate because steady state is made only if oxide formation and oxide destruction rate are same, from which oxide dissolution rate constant, k_s, was quantitatively obtained utilizing experimental data. Commonly observed current-time behavior, $i \propto t^m$, where m is different from 1 or 0.5, for passive film formation can be accounted for by virtue of enhanced oxide dissolution in high temperature aqueous environment.

1. Introduction

Alloy 600 has been used as the common constructing materials of control rod driving mechanism (CRDM) nozzle in PWR, which guides the control rod in reactor pressure vessel, due to the good general corrosion resistance in high temperature aqueous environment. But recently numbers of Environmentally Assisted Cracking (EAC, usually circumferential crack) have been observed in the inner diameter of CRDM nozzle near the weldment of CRDM nozzle and reactor pressure vessel head. It has given rise to severe problems in the safety of operating nuclear power plant.[1]

Currently as one of the possible solution of this problem, nickel plating is considered

in the inner diameter of CRDM nozzle to form stable passive oxide film, which is more resistant to EAC. This phenomenon is considered as closely related to the characteristics of oxide films formed on the alloy surface in high temperature aqueous environment, and it is generally believed that we can prevent or at least delay the speed of EAC by forming more stable oxide film.

Therefore it is natural that the passive oxide growth mechanism in this high temperature aqueous condition should be primary concern for the successful application. So far, as the passive film growth mechanism at room temperature, point defect model gains considerable attention for the growth, breakdown, and impedance characteristics of passive films on various metal surfaces, developed by Macdonald et al.[2-8] Based on this model, a new oxide growth law was derived to explain the passive film growth of nickel, especially oxide dissolution behavior in high temperature aqueous environment.

According to point defect model,[2-8] during the film growth, cation vacancies are produced at the film/solution interface but are consumed at the metal/film interface. Similarly, anion vacancies are formed at the metal/film interface but are consumed at the film/solution interface. Each point defect moves through the film by the chemical and electrical potential gradient inside the barrier layer film. Overall schematic diagram for passive nickel oxide formation process is depicted in Figure 1 reproduced from reference 5.[5-7]

Some calculations indicate nickel monoxide, NiO is not stable species below 200 ^{o}C, due to the stability of the hydroxide form, $Ni(OH)_2$[9]. Consequently, at 290 ^{o}C, which is experimental condition, NiO will grow rather than $Ni(OH)_2$ on pure nickel surface because NiO is more stable species.

2. Growth Law for Passive Film

In Figure 1 reactions (1) and (3) account for the consumption and formation of cation vacancies at the metal/film (m/f) interface and film/solution (f/s) interface, respectively, whereas reactions (2) and (4) describe similar phenomena related to anion vacancies. Reaction (5) explains the irreversible dissolution of the film at the barrier film/solution interface.[5-7]

In Figure 1, reactions (1), (3), and (4) are lattice conservative process, because they don't result in the movement of the barrier layer boundaries relative to a fixed reference frame, whereas reactions (2) and (5) are nonconservative. Therefore, reaction (2) describes film formation but reaction (5) is related to film destruction

process.[5-7] Accordingly corresponding oxide growth rate for these processes can be written as follows.[5-7]

$$\frac{dL_+}{dt} = -\Omega_f J_O]_{m/f} \qquad \frac{dL_-}{dt} = k_s \Omega_f C_{H^+}^n]_{f/s} \tag{1}$$

where $L, \Omega_f, J_O, C_{H^+}, k_s, n$ are film thickness, molar volume of oxide, oxygen vacancy flux inside film, concentration of hydrogen ion, dissolution rate constant and kinetic order of dissolution reaction respectively. The sign +, - denotes the oxide formation(oxide thickness increase) and destruction(oxide thickness decrease).

Analyzing two relations in Eq. (1), passive film growth rate can be described as,[5-7]

$$\frac{dL}{dt} = \frac{dL_+}{dt} - \frac{dL_-}{dt} = -\Omega_f J_O]_{m/f} - k_s \Omega_f C_{H^+}^n]_{f/s} \tag{2}$$

And current for oxide film growth is given by,[5]

$$i = 2F(J_M - J_O) \tag{3}$$

where J_M represents cation vacancy flux inside film.

According to point defect model, it is possible to calculate the diffusion rate of a charged species in the presence of both concentration and potential gradient, assuming that vacancy flux across the film are constant and component and self-diffusivity are same. The result is described as below.[2]

$$J_O = -2KD_O \frac{C_O]_{m/f} e^{2KL} - C_O]_{f/s}}{e^{2KL} - 1} \tag{4}$$

$$J_M = 2KD_M \frac{C_M]_{f/s} e^{2KL} - C_M]_{mlf}}{e^{2KL} - 1} \tag{5}$$

where C_O, C_M, K are the concentration of oxygen vacancies, concentration of cation vacancies and Fe/RT respectively. e is the electric field strength inside film.

Concentrations of vacancies at the interface can be calculated by considering interfacial equilibria in each reaction with Schottky-pair reaction.[2]

$$Null = V_{Ni^{"}} + V_{O^{\cdot\cdot}} \tag{6}$$

In point defect model the electrical potential drop across the film/solution interface is assumed to be[2]

$$f_{f/s} = f_{f/s}^o + aV + bpH \tag{7}$$

where a, b are the coefficients of potential drop dependence at film/solution interface on the external voltage and pH respectively.

From the relation,[2]

$$V + f_R = f_{m/f} + f_f + f_{f/s} \tag{8}$$

where f_R means potential drop at the reference electrode, the potential drop in metal/film interface can be derived as,[2]

$$f_{m/f} = (1-a)V - bpH - f^{o}_{f/s} + f_R - eL \tag{9}$$

where e is the electric field strength inside film, which is assumed to be constant as film thickens.[9]

Now the concentrations of vacancies at the interface is given by,[2]

$$C_O]_{m/f} = \frac{1}{\Omega_f}\exp\left(\frac{2Ff_{m/f} - \Delta G_2}{RT}\right) \tag{10}$$

$$C_{O(f/s)} = \frac{1}{\Omega_f}\exp\left(\frac{\Delta G_4 - 2Ff_{f/s}}{RT} - 4.406\,pH\right) \tag{11}$$

$$C_{M(m/f)} = \frac{1}{\Omega_f}\exp\left(\frac{\Delta G_1 - 2Ff_{\ m/f}}{RT}\right) \tag{12}$$

$$C_{M(f/s)} = \frac{1}{\Omega_f}\exp\left(\frac{2Ff_{\ f/s} - \Delta G_s - \Delta G_4}{RT} + 4.606\,pH\right) \tag{13}$$

where ΔG_k is the Gibbs free energy change of each reaction in Figure 1.

Replacing Eq. (4) and (5) with these relations, vacancy flux within the oxide becomes,[2]

$$J_O = -\frac{A(B-1)}{\Omega_f(e^{2KL}-1)} \tag{14}$$

$$J_M = \frac{2KD_{Ni}}{\Omega_f}\cdot\frac{e^{2KL}}{e^{2KL}-1}\cdot H \tag{15}$$

where,

$$A = 2KD_{V_O^{\cdot\cdot}}\exp\left[-\frac{2F}{RT}(aV + bpH + f_{f/s}{}^{o}) + \frac{\Delta G_4}{RT} - 4.606\,pH\right] \tag{16}$$

$$B = \exp\left[\frac{2F}{RT}(V + f_R) - \frac{\Delta G_2 + \Delta G_4}{RT} + 4.606\,pH\right] \tag{17}$$

$$H = \exp\left(\frac{2Fa\,V + 2Fb\;pH + 2Ff^{o}_{f/s} - \Delta G_s - \Delta G_4}{RT} + 4.406\,pH\right) - \exp\left(\frac{\Delta G_1 - 2F(1-a)V + 2Fb\;pH + 2Ff^{o}_{f/s} - 2Ff_{R}}{RT}\right) \quad (18)$$

The rate constant for oxide destruction reaction (5), and pH of the solution can be assumed constant throughout oxide formation process because for nickel oxide dissolution is not activated process.[6]

Then, the oxide growth rate can be written as follows.

$$\frac{dL}{dt} = \frac{A(B-1)}{\exp(2KL)-1} - k_s{}^{o}\Omega_f C^{n}_{H^+}]_{f/s} \quad (19)$$

If the oxide thickness does not change with time, that is, dL/dt = 0, steady state for oxide growth is attained and at this point, steady state thickness of oxide film, L_{ss}, can be calculated as follows.

$$L_{ss} = \frac{1}{2K}\ln(d+1) \approx \frac{1}{2K}\ln d \quad (20)$$

where

$$d = A(B-1)/k_s{}^{o}\Omega_f C^{n}_{H^+}]_{m/f} >>> 1 \quad (21)$$

Eq. (21) always holds when passive film of moderate steady state thickness forms on metal surface. After some calculations, the expression for oxide growth, Eq. (19), when moderate dissolution exists, can be integrated to following form.

$$L = \frac{1}{2K}\ln\left(1 + d[1-e^{-lt}]\right) \quad (22)$$

where

$$l = 2Kk_s\Omega_f C^{n}_{H^+}]_{f/s} \quad (23)$$

But except the very initial state of oxidation, Eq. (22) can be rewritten as follows.

$$L = \frac{1}{2K}\left[\ln d + \ln(1-e^{-lt})\right] = L_{ss} + \frac{1}{2K}\ln(1-e^{-lt}) \quad (24)$$

Here δ is dimensionless parameter and the ratio of oxide formation and destruction rate, related to the steady state oxide thickness whereas λ is related to dissolution rate.

The expression for the current of oxide growth becomes,

$$i = 2F(J_M - J_O) = 2F\left[\frac{2KD_M}{\Omega_f}\cdot\frac{e^{2KL}}{e^{2KL}-1}\cdot H + \frac{A(B-1)}{\Omega_f(e^{2KL}-1)}\right] \approx i_M + \frac{i_{ss}}{1-e^{-lt}} \quad (25)$$

where i_M, i_{ss} are described as,

$$i_M = \frac{4FKD_M}{\Omega_f}\cdot\frac{e^{2KL}}{e^{2KL}-1}\cdot H \approx \frac{4FKD_M H}{\Omega_f} \quad (26)$$

$$i_{ss} = \frac{2FA(B-1)}{\Omega_f e^{2KL_{ss}}} = \frac{2FA(B-1)}{\Omega_f d} \quad (27)$$

i_M, i_{ss} are the cation transmission current through the oxide film and steady state current for passive oxide formation respectively.

Therefore we can quantify the effect of dissolution to steady state oxide thickness and current measured referring to Eq. (24) and (25). If dissolution rate of one material is l times that of another, the other conditions being all same, steady state thickness becomes smaller by $(1/2K)\ln l$ and steady current increases l times that of another material. And the flux of cation vacancies in the film contributes to total current by forming constant ambient current. We can measure dissolution rate constant of oxide films if we compare experimental data with the Eq. (24) and (25).

When dissolution rate is very small, exponential term in Eq. (24) and (25) can be series expanded, and after some manipulations, the result is,

$$L = \frac{1}{2K}\left[\ln 2KA(B-1) + \ln t\right] \quad (28)$$

$$i = i_M + \frac{F}{K\Omega_f}\cdot t^{-1} \quad (29)$$

These two equations exactly coincide with originally induced equations in point defect model at Macdonald et al's work,[2] that is, oxide growth follows logarithmic growth law and current is inversely proportional to oxidation time.

3. Experiment

Potentiostatic polarization experiment for Alloy 600 and electrolytic nickel-plated Alloy 600 was performed in high temperature aqueous environment simulating PWR primary side. Alloy 600 was obtained from commercial source. The bulk material was cut with electric discharge machining (EDM) and the oxide layer formed during EDM was eliminated with SiC papers. One of the specimens was electrolytically nickel-plated

with thickness 30 μm whereas the other one is polished with 3 μm alumina powders. Lithium hydroxide and boric acid was added to set 2 ppm of lithium and 1000 ppm of boron. The pH of the solution was calculated as 6.86 using commercial software whereas neutral pH at 290 °C was calculated as 5.63. Temperature and pressure was maintained at 290 °C and 140 atm. As a reference electrode, Ag/AgCl external electrode was used and platinized platinum electrode as counter electrode. Solatron 1286 and HP VEE® was used for experimental apparatus and data acquisition. At 290 °C and pH 6.86, the equilibrium potential for nickel oxide formation reaction was calculated as –728 mV versus SHE(T=298 °C).[10,11]

$$Ni + H_2O = NiO + 2H^+ + 2e^- \quad (30)$$

Potentiostatic polarization with overvoltage +129 mV versus equilibrium potential of nickel oxide formation was applied for each specimen and the current transient was recorded.

4. Results and Discussion

In the conventional point defect model, the current transient for the potentiostatic oxide formation is predicted to be subject to following two relations.[2]

$i \propto t^{-1}$ for ordinary oxide film (31)

$i \propto t^{-1/2}$ for extremely thin film (32)

But the current when there is non-negligible oxide dissolution and cation transmission current is expressed as Eq. (33) according to the derivation based on point defect model.

$$i = i_M + \frac{i_{ss}}{1 - e^{-lt}} \quad (33)$$

In Eq. (33), cation transmission current contributes to the total current measured experimentally by forming constant base current. And the current for anion vacancy flux decreases to i_{ss} with time. The speed of passivation is related to the parameter λ. For example, if λ is large, slow or little passivation will occur.

The current transient curve for potentiostatic polarization of each specimen was plotted in Figure 2. As shown in the figures, the current for oxide formation for nickel-plated Alloy 600 is observed as substantially greater than conventional point defect model predicts. That is, typical m for the current-time behavior of Eq. (34) for the potentiostatic polarization of plated nickel,

$$i \propto t^{-m} \quad (34)$$

was determined as 0.24 whereas that of Alloy 600 was 0.62. This means that there

occurs very slow passivation of nickel surface of plated Alloy 600 compared with that of bare Alloy 600 or the common passive films at room temperature. The calculated data are listed in Table 1. This can be explained in two aspects.

Firstly, cation vacancy flux can affect the estimated m values because constant ambient current has a tendency to assume somewhat lower value of m in the fitting process of the experimental data.

Secondly, oxide dissolution can delay oxide growth and change oxide growth mechanism and may be responsible for considerable amount of total current measured. If severe oxide dissolution occurs, the steady state thickness of oxide will be smaller and the steady state current will be larger because of higher flux of oxygen vacancies across oxide film. In Eq. (33), the dissolution parameter λ can be obtained by changing the equation slightly to following form.

$$l \propto -(1/t)\ln(1-i_{ss}/i) \tag{35}$$

But in Eq. (35), errors can be introduced from the uncertainties in the values of steady state current, the effect of cation transmission current, and the interface limiting flux of vacancies at the initial state of the oxide growth. Figure 3 shows the plots of Eq. (35) for each of the specimen. The measured λ are listed in Table 2. And oxide dissolution rate constant can be calculated using following equation.

$$k_s = \frac{l}{2K\Omega_f C^n{}_{H^+}]_{f/s}} = \frac{i_{ss}}{2FC^n_{H^+}]_{f/s}} = \frac{i_{ss}}{2F}\cdot 10^{-n\cdot pH} \tag{36}$$

where

$$i_{ss} = \frac{2FA(B-1)}{\Omega_f d} = \frac{Fl}{K\Omega_f} \tag{37}$$

By this analysis, oxide dissolution rate constant is closely related to the steady state current because steady state is accomplished only when film formation rate and oxide dissolution rate are same.

Assuming kinetic order n for oxide dissolution reaction,

$$NiO + 2H^+ \xrightarrow{k_s} Ni^{++} + H_2O \tag{38}$$

is 2 and considering measured steady state current and estimated solution pH, calculated dissolution rates are also listed in Table 2. As shown in the table, the dissolution rate constant of nickel-plated Alloy 600 oxide is larger than that of Alloy 600. This is consistent with the fact that m value of nickel-plated Alloy 600 is smaller than that of Alloy 600. Therefore small m value for nickel-plated Alloy 600 in high temperature aqueous environment is closely related with cation transmission current and enhanced oxide dissolution at that temperature. In both cases, corrosion of metal is expected to increase and passivation of metal surface to be retarded. This may account

for the behavior that for nickel a critical temperature for loss of passivity exists and is in the range of 75 - 150 ^{o}C, which is known as a function of both the scanning direction and the solution pH.[10] Hence we conclude that the passivation ability of plated nickel in this environment is inferior to that of Alloy 600. But according to Pourbaix diagram for nickel at 290 ^{o}C, nickel is actually in the corrosion-immune region in PWR primary environment because the equilibrium potential of nickel oxide formation, NiO, is more positive than that of water stability for hydrogen evolution[10]. This means that corrosion of pure nickel, let alone nickel oxide, in this environment is thermodynamically impossible. Therefore the stability of nickel oxide in PWR primary environment has close relationship with the electrochemical noble character of nickel.

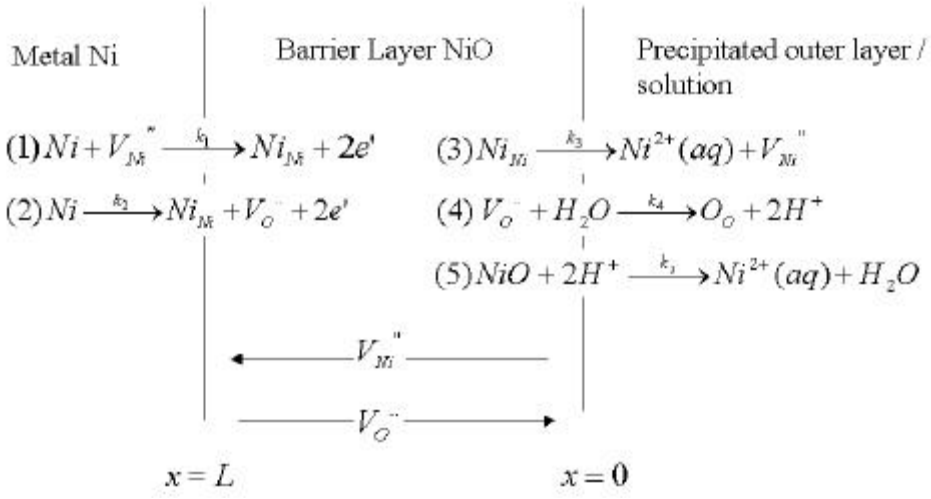

Figure 1. Schematic diagram for the oxide growth process that occur within nickel passive oxide film according to point defect model (Reproduced from reference 5)

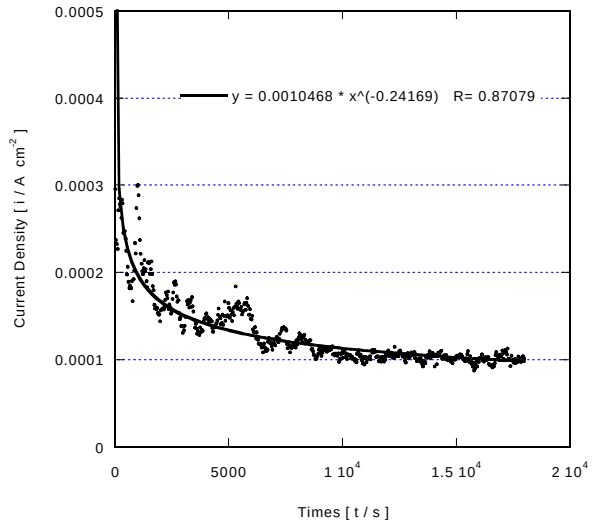

(a)

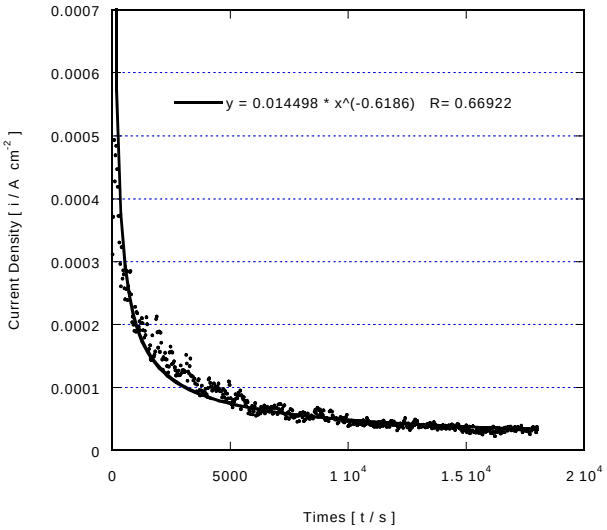

(b)

Figure 2. Potentiostatic polarization curve for (a) electrolytic nickel-plated Alloy 600 with 30 μm, and (b) bare Alloy 600 in Li = 2 ppm, B = 1000 ppm, pH = 6.86 at 290 ^{o}C. *neutral pH at 290 ^{o}C = 5.63

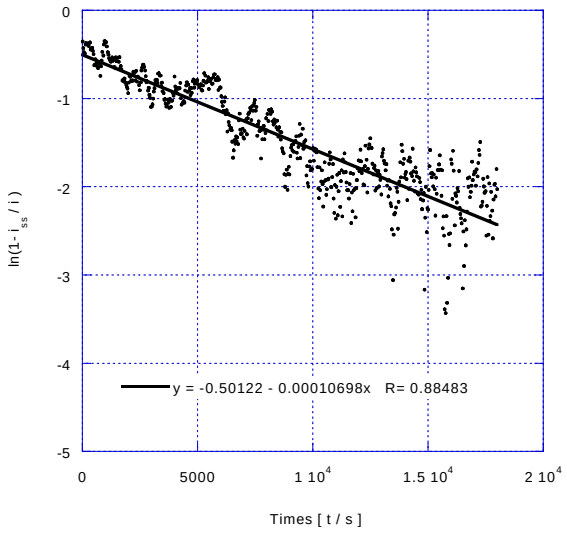

(a)

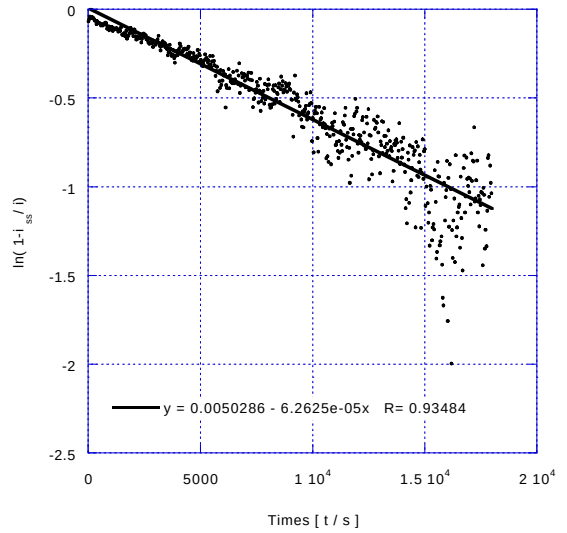

(b)

Figure 3. Logarithmic current behavior with time according to the new developed oxide growth law for (a) electrolytic nickel-plated Alloy 600 with 30 μm, and (b) bare Alloy 600 in Li = 2 ppm, B = 1000 ppm, pH = 6.86 at 290 °C.

Table 1. m for $i \propto t^{-m}$ in potentiostatic polarization curve

Specimen	Nickel-plated Alloy 600	Alloy 600
m for $i \propto t^{-m}$	0.24	0.62

Table 2. Estimated dissolution rate constant of specimens

Specimen	Nickel-plated Alloy 600	Alloy 600
$\lambda \times 10^5$ / s^{-1}	10.7	6.26
i_{ss} / $\mu A\ cm^{-2}$	102	33
$k_s \times 10^{24}$ / $mol\ cm^{-2}\ s^{-1}$	10.1	3.26

5. Conclusion

The passive film growth law for nickel was improved to include oxide dissolution rate compared with conventional point defect model to explain retarded passivation of nickel found in PWR primary environment. According to this model, oxide growth and its passivation current transient is closely related with oxide dissolution rate because steady state is established only if oxide formation and oxide destruction rate are same, from which oxide dissolution rate constant k_s was quantitatively obtained. Commonly observed current-time behavior, $i \propto t^m$, where m is different from 1 or 0.5, was also accounted for in the light of enhanced oxide dissolution in high temperature aqueous environment. As a result, the passivation speed of plated nickel was slower than that of Alloy 600 and passivation current of plated nickel was greater than that of Alloy 600. Therefore we conclude that the good applicability of nickel-plating for PWR primary environment is due to its inherent electrochemically noble character in this environment, not due to its passivation ability.

References

[1] Y. Colot, C. Pichon, Vessel Head Penetrations Cracking in French PWRs, Proceedings of 1992 EPRI Workshop on PWSCC of Alloy 600 in PWRs, Electric Power Research Institute(EPRI) TR-103345, Dec. 1993.

[2] C. Y. Chao, L. F. Lin, D. D. Macdonald, J. Electrochem. Soc. **128** (1981) 1187.

[3] C. Y. Chao, L. F. Lin, D. D. Macdonald, J. Electrochem. Soc. **128** (1981) 1194.

[4] C. Y. Chao, L. F. Lin, D. D. Macdonald, J. Electrochem. Soc. **129** (1982) 1874.

[5] D. D. Macdonald, M. Urquidi-Macdonald, J. Electrochem. Soc. **137** (1990) 2395.

[6] D. D. Macdonald, S. R. Biaggio, H. Song, J. Electrochem. Soc. **139** (1992) 170.

[7] D. D. Macdonald, J. Electrochem. Soc. **139**, (1992) 3434.

[8] L. Zhang, D. D. Macdonald, Electrochimica Acta. **43** (1998) 679.

[9] B. Beverskog, I. Puigdomenech, Corrosion Science **38** (1996) 2121

[10] R. L. Cowan, R. W. Staehle, J. Electrochem. Soc. **118** (1971) 557.

[11] M. Pourbaix, Atlas of electrochemical equilibria in aqueous solutions, 2nd English ed., National Association of Corrosion Engineers, 1974.